DYNAMIC STABILITY STUDIED OF AN INTEGRATED WIND AND SOLAR ENERGY GENERATION TO POWER GRID

NGHIÊN CỨU ỔN ĐỊNH ĐỘNG TRONG HỆ THỐNG ĐIỆN TÍCH HỢP NĂNG LƯỢNG GIÓ VÀ NĂNG LƯỢNG MẶT TRỜI

Truong Dinh Nhon, Nguyen Thi Mi Sa, Nguyen Minh Chon
Ho Chi Minh City University of Technology and Education

Received 16/01/2017, Peer reviewed 22/01/2017, Accepted for publication 17/02/2017

ABSTRACT

This paper proposes an integrated renewable power generation system including wind power and solar power which are connected to a commercial power system through the same DC bus. The wind power generators are based on the Permanent Magnet Synchronous Generator (PMSG). Different power sources can be interconnected anywhere on the same DC power line, leading to flexible system expansion. A time-domain scheme based on a nonlinear system model subject to a permanent DC fault in one of the DC links is systematically performed to evaluate the dynamic stability of the studied power system.

Keywords*: Wind power, solar power, PMSG, hybrid, dynamicstability*

TÓM TẮT

Bài báo đề xuất hệ thống phát điện tích hợp năng lượng mới bao gồm năng lượng gió và năng lượng mặt trời nối với lưới điện thông qua hệ thống bus DC chung. Năng lượng gió sử dụng máy phát điện đồng bộ nam châm vĩnh cửu (PMSG). Các nguồn phát điện khác nhau có thể nối vào bất kỳ vị trí nào trong hệ thống điện 1 chiều thể hiện tính linh hoạt trong việc mở rộng hệ thống điện. Kết quả mô phỏng trong miền thời gian dựa vào mô hình phi tuyến của hệ thống khi cho sự cố vĩnh viễn ở một trong các bus DC hệ thống được thực hiện để đánh giá độ ổn định động của hệ thống nghiên cứu.

Từ khóa: *Năng lượng gió, năng lượng mặt trời, máy phát điện đồng bộ nam châm vĩnh cửu, kết hợp, ổn định động.*

1. INTRODUCTION

Renewable-energy issue is one of the hottest topics in the whole world today due to the fast and huge consumption of fossil fuels. Renewable energy can be derived from several resources such as solar, wind, ocean waves, water flow and tides, geothermal heat, biological sources…[1]. Among these resources, wind power is now a very mature and established renewable energy throughout the world. The use of wind power is increasing at an annual rate of 20%, with a worldwide installed capacity of 238,000 MW at the end of 2011[2]. However, other renewable energies such as photovoltaic (PV) energy also have significant potential. In 2004, PV energy passed wind energy to be the fastest growing energy resource and since 2007 it has been more than doubled every two years. The photovoltaic capacity worldwide was 67,000 MW at the end of 2011 [3].

In practice, a hybrid wind and PV energy system can reliably supply a part of the world's

energy needs, with significant benefit to climate, air quality, water quality, ecological systems, and energy security, at reasonable cost [4-6].

Nowadays, hybrid system is mainly composed of natural energy sources, and in some cases, it can be incorporated into the system with traditional energy sources like coal and gas as well. However, there is a tendency that the greater the system sophistication, the more suitable the power control techniques are required to be. For more details, in [7] the development of Stand Alone hybrid Wind-Solar Photovoltaic system where energy storage device is used for voltage control is proposed. Moreover, a complete evaluation system of wind power integration capacity has also been proposed by defining the evaluation index system after considering the plant capacity of power grid, the scale of the power grid, the level of load, the wind-solar complementary characteristics, and the capacity of flexible load [8].

This paper presents the dynamic stability evaluation of the integrated wind and PV power generation system fed to power system under various operating conditions. Time-domain schemes based on nonlinear system models subject to disturbance are carried out to evaluate the response of the proposed system.

2. CONFIGURATION OF THE STUDIED SYSTEM

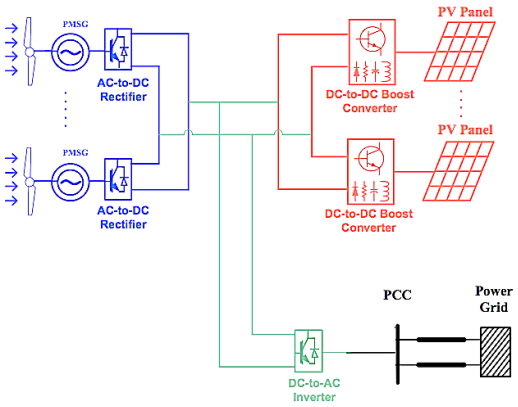

***Figure 1**. Configuration of the studied system*

Fig.1 illustrates a schematic diagram of the proposed integrated generation consisting of four subsystems: a wind generation subsystem, a solar generation subsystem, an interface subsystem and a power system. The four subsystems share their DC links.

In the wind generation subsystem, the 5x2-MW wind turbines are represented by five permanent magnet synchronous generators (PMSG) driven by five variable-speed wind turbines (VSWT) and five rectifiers. The converter is used to control indirectly the operating point of the wind turbine by commanding the rotor speed and the voltage on the PMSG terminals. The dynamic behavior of the wind generation subsystem can be characterized by two nonlinear differential equations involving the *d*- and *q*-axis modulation indices of the VSC-converter. For the detailed mathematic description of the wind subsystem, please refer to [9].

In the 5x1.5-MW solar generation subsystem, there are five photo-voltaic (PV) panel arrays and five half-bridge boost DC-DC converters. Similar to the wind subsystem, the converter is used to control the operating point of the PV panels. The dynamic behavior of the solar generation subsystem can be characterized by two nonlinear equations involving the voltage level on the DC-DC converters and the current injected into the DC bus.

These two subsystems are interconnected at the output sides of individual converters and are also connected to the DC-AC inverter through interface subsystem. This inverter converts wind and solar energy generated by these sources useful to costumers.

Three subsystems including wind, solar and interface are also connected to the PCC of the traditional power system.

The employed mathematical models of the studied system are described as below. The equations in the following subsections are expressed in per unit (pu) except that the time variable *t* and base angular frequency ω_b are in s and rad/s, respectively.

2.1 Variable-Speed Wind Turbine

The captured mechanical power P_{mw} (in W) by a VSWT from wind is given by

$$P_{mw} = \frac{1}{2}\rho_w \cdot A_{rw} \cdot V_w^3 \cdot C_{pw}(\lambda_w, \beta_w) \quad (1)$$

where ρ_w is the air density (kg/m^3), A_{rw} is the blade impact area (m^2), V_w is the wind speed (m/s), and C_{pw} is the dimensionless power coefficient of the VSWT. The expression for C_{pw} is depicted by

$$C_{pw}(\gamma_{kw}, \beta_w) = c_1\left(\frac{c_2}{\gamma_{kw}} - c_3\beta_w - c_4\beta_w^{c_5} - c_6\right)\exp\left(-\frac{c_7}{\gamma_{kw}}\right) \quad (2)$$

in which

$$\frac{1}{\gamma_{kw}} = \frac{1}{\lambda_w + c_8 \cdot \beta_w} - \frac{c_9}{\beta_w^3 + 1} \quad (3)$$

$$\lambda_w = \frac{R_{bw} \cdot \omega_{bw}}{V_w} \quad (4)$$

Where ω_{hw} is the blade angular speed (rad/s), R_{bw} is the blade radius (m), λ_w is the tip speed ratio, β_w is the blade pitch angle (degrees), and c_1-c_9 are the constant coefficients of C_{pw} of the studied VSWT. The cut-in, rated, and cut-out wind speeds of the VSWT are 4,14, and 24m/s, respectively.

2.2 PMSG Model and Operation of Power Converters

The *d-q* axis equivalent circuit model of the studied wind PMSG can be expressed by [6]

$$p(\phi_{qw}) = \omega_b v_{qsw} + \omega_b r_{sw} i_{qsw} - \omega_{rw}\phi_{dw} \quad (5)$$

$$p(\phi_{dw}) = \omega_b v_{dsw} + \omega_b r_{sw} i_{dsw} + \omega_{rw}\phi_{qw} \quad (6)$$

in which

$$\phi_{qw} = -(X_{mqw} + X_{lsw})i_{qsw} = -X_{qw} i_{qsw} \quad (7)$$

$$\begin{aligned}\phi_{dw} &= -(X_{mdw} + X_{lsw})i_{dsw} + X_{mdw} i'_{mw} \\ &= -X_{dw} i_{dsw} + X_{mdw} i'_{mw}\end{aligned} \quad (8)$$

where ϕ is the pu flux linkage, v_{sw} is the pu stator-winding voltage, i_{sw} is the pu stator-winding current, X_{mw} is the pu magnetization reactance, X_{lsw} is the pu leakage reactance, i'_{mw} is the pu magnetization current, and ω_{rw} is the pu rotational speed of the studied PMSG.

The input *d-q* axis pu voltages of the i^{th} VSC-converter of the PMSG can be expressed by $v_{condwi} = km_{condwi} v_{dc}$ and $v_{conqwi} = km_{conqwi} v_{dc}$, respectively, where v_{dc} is the DC-link voltage while km_{condwi} and km_{conqwi} are the *d*- and *q*-axis modulation indices of the i^{th} VSC-converter, respectively.

The fundamental control block diagrams of the VSC-based converter of each of the wind PMSG can be referred to [8]. In which, km_{condw} is employed to control the rotor speed of the wind PMSG (ω_{rw}), and km_{conqw} is utilized to control the stator-winding voltage of the PMSG (v_{sw}).

2.3 Model for PV System

Each practical PV panel of the studied system has the following specifications: BP275UU, rated power of 75 W, rated voltage of 17 V, rated current of 4.45 A, open-circuit voltage of 21.4 V, and short-circuit current of 4.5 A. Since the output voltage of PV cell is very low, a number of PV cells are connected together in series in order to obtain required higher voltages. A number of PV cells are put together and encapsulated with glass, plastic, and other transparent materials to protect against harsh environments and a PV module can then be formed. To obtain the required voltage and power, a number of modules are

connected in parallel to form a PV array. Fig.2 shows an equivalent circuit diagram of a PV array including an equivalent short-circuit current source I_{SC} in parallel with a diode and a shunt resistor R_{sh}, where N_s is the number of cells in series and N_p is the number of modules in parallel. The equivalent-circuit model of the PV array shown in Fig.2 can be expressed by the following equations:

$$I_{PV} = N_p I_{SC} - N_p I_D \left\{ \exp\left[\frac{q}{AkT}\left(\frac{V_{R\_PV}}{N_s} + \frac{R_S I_{PV}}{N_p}\right)\right] - 1 \right\} - \frac{N_p}{R_{sh}}\left(\frac{V_{PV}}{N_s} + \frac{R_S I_{PV}}{N_p}\right) \quad (9)$$

where V_{R_PV} is the output voltage of the PV array, q is the charge of an electron (q = -1.602×10^{-19} C), k is Boltzmann constant (k = 1.38 ×10^{-23} J/K), T is temperature in K, A is the quality factor which is a constant, I_D is the reverse saturation current of the diode, and I_{SC} is the short-circuit current under the solar radiation of 1000 W/m^2.

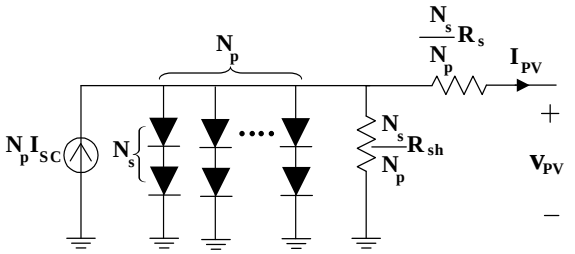

Figure 2. *Equivalent circuit of the studied PV array*

Fig.3 shows that the output voltage of the PV array is fed to an DC-DC boost converter to step up the PV voltage to a higher level.

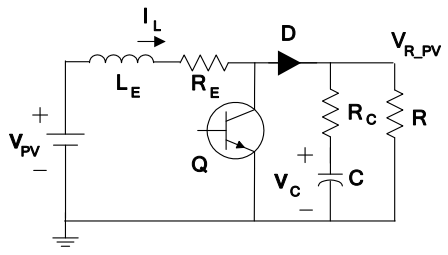

Figure 3. *The equivalent circuit of DC-to-DC boost converter.*

The DC line from the output of the boost DC-DC converter to the input of the DC-AC inverter is represented by an equivalent T circuit as shown in Fig.4. The capacitor C_{DC}, which is located at the midpoint of the DC line, can be considered as a battery model for energy storage. The dynamic equations of DC-DC boost converter can be expressed by the following equation:

$$\begin{bmatrix} p(I_L) \\ p(V_C) \end{bmatrix} = \begin{bmatrix} -\frac{R_E + (1-D)(R//R_C)}{L_E} & -\frac{(1-D)R}{L_E(R+R_C)} \\ \frac{(1-D)R}{(R+R_C)C} & -\frac{1}{(R+R_C)C} \end{bmatrix} \begin{bmatrix} I_L \\ V_C \end{bmatrix} + \begin{bmatrix} \frac{1}{L_E} \\ 0 \end{bmatrix} V_{PV} \quad (10)$$

$$V_{R\_PV} = \left[(1-D)(R_C // \frac{R}{R+R_C} \right] \begin{bmatrix} I_L \\ V_C \end{bmatrix} \quad (11)$$

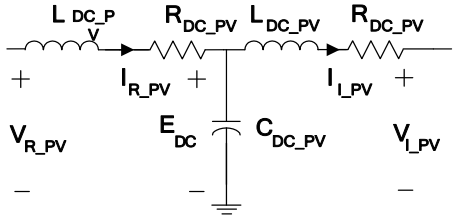

Figure 4. *The equivalent circuit of DC line in PV array*

According to Fig.4, the pu differential equations of the DC line can be described by

$$(L_{DC\_PV})\,p(I_{R\_PV}) = V_{R\_PV} - R_{DC\_PV} I_{R\_PV} - E_{DC} \quad (12)$$

$$(C_{DC\_PV})\,p(E_{DC}) = I_{R\_PV} - I_{I\_PV} \quad (13)$$

$$(L_{DC\_PV})\,p(I_{I\_PV}) = E_{DC} - V_{I\_PV} - R_{DC\_PV} I_{I\_PV} \quad (14)$$

$$T_{kminv}.p(\Delta km_{inv}) = K_{kminv}(Q_{w\_pv,ref} - Q_{w\_pv}) - \Delta km_{inv} \quad (15)$$

$$T_{\delta inv}.p(\Delta\delta_{inv}) = K_{\delta inv}(V_{dc\_ref} - V_{dc}) - \Delta\delta_{inv} \quad (16)$$

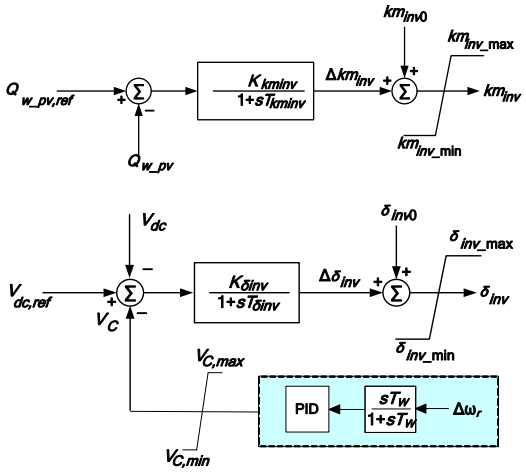

Figure 5. *Control block diagram of DC-to-AC inverter of hybrid system.*

where Δ represents the quantities of deviation, subscript *ref* denotes the quantities of reference,K_{km} and K_{δ} are the gains of the modulation index control block and the phase angle control block of the inverter, respectively; and T_{km} and T_{δ} are the time constants of the modulation index control block and the phase angle control block of the inverter, respectively.

2.4 Interface Subsystem

The DC bus collects the energy generated by both the wind and solar subsystems and delivers it to the utility.

The output *d-q* axis pu voltages of the VSC-inverter of the hybrid system (wind and solar generation) can be written by

$$v_{invd} = km_{inv}\sin(\alpha_{inv})v_{dc} \quad (17)$$

$$v_{invq} = km_{inv}\cos(\alpha_{inv})v_{dc} \quad (18)$$

where km_{inv} and δ_{inv} are the modulation index and the phase angle of the VSC-inverter, respectively. In which, δ_{inv} is responsible to control the DC-link voltage (v_{dc}), km_{inv} is used to control the output reactive power of the hybrid system (Q_{w_pv}), km_{condw} is employed to control the rotor speed of the wind PMSG (ω_{rw}), and km_{conqw} is utilized to control the stator-winding voltage of the PMSG (v_{sw}) [7].

3. TIME-DOMAIN SIMULATIONS

This section employs the nonlinear-system model developed in Section 2 to evaluate the stability of the studied system under a permanent DC fault in one of the DC links of wind generation subsystem side. It is assumed that the OWF operates under a wind speed V_W of 12 m/s, the PV array operates under the irradiance of 1000 W/m^2, the short-circuit current I_{SC} of 7.77 A, and the diode's reverse saturation current I_D of 9×10^{-11} A.

If there is a permanent DC fault in one of the DC links of wind generation subsystem side in studied system, it may lead to lose of one wind farm. It is similar to the fact that one wind farm is tripped out of the system. To test this scenario, the studied system is subjected to a permanent fault at the middle of DC link 1 at t = 5s. The transient responses of the remaining system are presented in Fig.6.

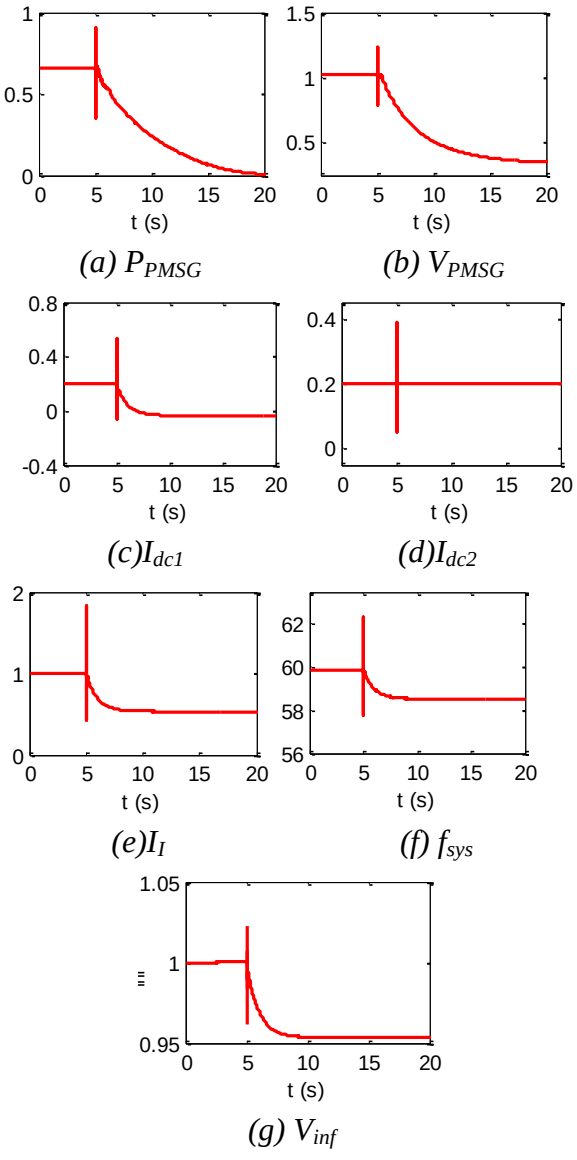

***Figure 6**. Transient responses of the studied system subject to a permanent DC fault at the middle of DC link 1*

Figs. 6(a) and (b) show the transient responses of the active-power, the terminal

voltage of the PMSG-based wind generations, the current of rectifier and inverter of the interface subsystem, the grid frequency, and the voltage at infinite bus, respectively. It can be seen that the power flow in the DC link 1 is zero after fault (Fig.6(e)). The other quantities such as the DC current of inverter, the grid frequency and the voltage at infinite bus can reach to the new steady-state conditions.

4. CONCLUSION

This paper has presented the transient stability evaluation of an integration of a WF and a PV system fed to power system through the same DC bus. The time-domain simulations of the studied system subject to a permanent DC fault in one of the DC links of wind generation subsystem side have been performed to evaluate the stability of the studied system.

REFERENCES

[1] U. Bossel - On the way to a sustainable energy future, *Proc. 27th International Telecommunications Conference (INTELEC)*, 18-22 Sep. 2005, Berlin, Germany 659-668.
[2] Renewables 2011 global status report, REN21, 15 Rue de Milan, Paris, 2011, pp. 1-115.
[3] European Photovoltaic Industry Association - Market report 2011, EPIA, Rue d'Arlon 63-67, 1040 Brussels, Belgium, 2012, pp. 1-34.
[4] M. A. Delucchi and M. Z. Jacobson - Providing all global energy with wind, water, and solar power, Part I: Technologies, energy resources, quantities and areas of infrastructure, and materials, *Energy Policy* 39 (3) (2011) 1154-1169.
[5] D.-N. Truong and L. Wang - Power system stability enhancement with an integrated offshore wind farm and marine-current farm using a STATCOM, *Proc. IEEE Asia Pacific Conference on Circuits and Systems*, 2-5 December 2012, Kaohsiung, Taiwan 571-574.
[6] M. A. Mahmud, H. R. Pota, and M. J. Hossain - Dynamic stability of three-phase grid-connected photovoltaic system using zero dynamic design approach, *IEEE Journal of Photovoltaics*, 2(4) (2012) 564-571.
[7] M. Y. Zargar, M. u. D. Mufti and S. A. Lone, "Modelling and control of wind solar hybrid system using energy storage system," *2016 International Conference on Computing, Communication and Automation (ICCCA)*, Noida, 2016, pp. 965-970.
[8] WenboHao, Chengzhi Sun and Zhao Leilei, "The research on adaptability evaluation of wind power integration capacity in power grid considering wind-solar hybrid complementary characteristics and flexible loads interference," *2016 IEEE PES Asia-Pacific Power and Energy Engineering Conference (APPEEC)*, Xi'an, 2016, pp. 1856-1860.
[9] C.-H. Lin, W.-L. Hsieh, C.-S. Chen, C.-T. Hsu, T.-T. Ku, and C.-T. Tsai - Financial analysis of a large-scale photovoltaic system and its impact on distribution feeders, *IEEE Trans. Industry Applications*, 47 (4) (2011) 1884-1891.

Corresponding author:
Dr. Truong Dinh Nhon
Ho Chi Minh City University of Technology and Education
Email: nhontd@hcmute.edu.vn